NBTI modeling in analog circuits and its application to long-term aging simulations

Kay-Uwe Giering,* Christoph Sohrmann,* Gerhard Rzepa,§ Leonhard Heiß,‡ Tibor Grasser,§ and Roland Jancke*
*Fraunhofer IIS Dresden, Germany §TU Wien, Austria ‡TU München, Germany

***Abstract*—We propose a circuit-level modeling approach for the threshold voltage shift in PMOS devices due to the negative-bias temperature instability (NBTI). The model is suitable for application in analog circuit design and reproduces the results of existing digital-stress NBTI models in the limit of two-level stress signals. It accounts for recovery effects during intervals of low stress, and it predicts a stress-pattern dependent saturation of the degradation at large operation times. Since the model can be solved numerically in an efficient way, we have direct access to the threshold voltage shift at arbitrary times, in particular to the exact solution at large operation times, without any approximation. We implement the model via the Cadence Spectre URI. Finally, we make use of the model to compare the aging properties of several analog stress patterns. We furthermore present the results of an analog circuit-level NBTI simulation of a ring oscillator.**

I. Introduction

The continuing miniaturization of electronics in the sub-micrometer regime has triggered an extensive research on the aging of PMOS devices due to NBTI. Sophisticated models for the microscopic processes causing NBTI aging are available and show a remarkable agreement with measurements [1], [2], [3], [4]: On the one hand, gate oxide defects reversibly trap charge carriers, thereby contributing to a recoverable degradation. On the other hand, oxide-substrate interface states are supposed to cause a degradation that is permanent on the typical experimental time scales. The accumulation of charge in or near the oxide layer reduces the MOSFET performance, for instance causes a decrease in the threshold voltage. These findings were mainly applied to digitally operated circuits [5], [6], [7] by means of so-called capture-emission-time (CET) maps. The parametrization of the CET map voltage dependence [8] led to a model for piecewise-constant stress at arbitrary voltage levels [9], [10]. References [11], [12] present a formally similar analog-NBTI approach but use different assumptions in the microscopic model and its solution. The defect-centric viewpoint [13] provides a complementary approach for small devices.

Analog-circuit MOSFETs mostly feature a large channel area and contain a number of BTI-relevant defects high enough such that the device-to-device variation is negligible and a statistical averaging over all traps is admissible. This statistics requires detailed information on the distribution of the defect time constants as well as on their stress voltage and temperature dependence. In the specific case of digital AC stress, where the stress voltage takes on the two values V_h (= on) and V_l (= off), the capture-emission-time map provides the relevant information and allows for a thorough analysis of this situation [5], [6], [7].

Corresponding author: kay-uwe.giering@eas.iis.fraunhofer.de

For analog stress voltages, the parametrization of a family of CET maps is needed. Reference [8] points out that a change in the stress voltage mainly leads to a shift of the CET map in the space of time constants, as well as to an overall amplitude factor split from the solution to the related master equation. Furthermore, two classes of defects are at work, each with an approximately Gaussian energy distribution profile [14]; the one exhibiting small time constants ("recoverable component") and the other one large time constants ("permanent component").

The stochastic charging and discharging of the individual defects contributing to NBTI is commonly modeled as a Markov process [3] with a positively charged and a neutral state. Averaging over many realizations of the stochastic process, the probability $w(t)$ of finding the defect in the positively charged state satisfies a master equation

$$\dot{w} = \frac{1}{\tau_c}\,(1-w) + \frac{1}{\tau_e}\,w, \qquad w(t_0) = w_0, \tag{1}$$

with hole capture and emission times τ_c and τ_e. The defect contributes to the NBTI threshold voltage shift as $V_{\text{th}}(t_2) - V_{\text{th}}(t_1) = \eta \cdot (w(t_2) - w(t_1))$, with η measuring the specific trap contribution. Notice that τ_c, τ_e and η are characteristic quantities of the individual trap, they furthermore depend on the external parameters such as stress voltage V_{gs} and temperature ϑ.

In the following two sections we present our analog-NBTI modeling approach and its solution from a mathematical point of view. We then continue with the details of our numerical implementation and finally discuss the simulation results for the aging of a single transistor and for the aging of a more complex circuit made up by several transistors.

II. Analog-stress NBTI model

The threshold voltage change due to the NBTI degradation is given as an integral in activation-energy space

$$V_{\text{th}}(t) = V_{\text{th}}^{\text{empty}} - \sum_r \int \mathrm{d}e_c \mathrm{d}e_e\ \Phi_r(e_c,e_e)\ w^{(r)}_{e_c,e_e,V_{\text{gs}}}(t). \tag{2}$$

Here, the defect distribution map Φ_r is a weighting factor for the statistical averaging over the high number of oxide traps or interface states present in a large PMOS device. Its two components $r = R, P$ correspond to the recoverable and permanent degradation mechanisms and are taken as Gaussian profiles [14]. Both constituents contribute independently to the threshold voltage shift $\Delta(t) := V_{\text{th}}^{\text{empty}} - V_{\text{th}}(t) \geq 0$ as $\Delta(t) = \Delta_R(t) + \Delta_P(t)$.

Multiplying Φ with the probability $w^{(r)}_{e_c,e_e,V_{\text{gs}}}(t)$ of finding the defect in the positively charged state provides the contribution of the defects with energies near (e_c, e_e) to $\Delta(t)$. The

 978-1-4799-7274-6/14/$31.00 ©2014 IEEE

stress-induced energy shifts are not encoded in Φ but in the independent functions $V_{\text{gs}} \mapsto \delta E_c^{(r)}, \delta E_e^{(r)}$: The specific process $w_{e_c,e_e,V_{\text{gs}}}(t)$ is subject to the activation energies $e_c + \delta E_c(V_{\text{gs}})$, $e_e + \delta E_e(V_{\text{gs}})$ for capture and emission, respectively. This results in the mean times for charge capture or emission

$$\begin{aligned} \tau_c^{(r)}(e_c, V_{\text{gs}}, \vartheta) &= \tau_{0,c}^{(r)}(V_{\text{gs}}) \ \exp\left[+\beta\big(e_c + \delta E_c^{(r)}(V_{\text{gs}})\big)\right], \\ \tau_e^{(r)}(e_e, V_{\text{gs}}, \vartheta) &= \tau_{0,e}^{(r)}(V_{\text{gs}}) \ \exp\left[+\beta\big(e_e + \delta E_e^{(r)}(V_{\text{gs}})\big)\right]. \end{aligned} \tag{3}$$

For analog gate-source voltages $V_{\text{gs}}(t)$, the capture and emission times of a single defect are time-dependent functions taking on continuous values. The factor β accounts for the temperature activation. In contrast to the modeling of Ref. [12], the experimental data available to us requires the prefactors τ_0 in (3) to be stress-dependent: in the voltage range -1.5V $\leq -V_{\text{gs}} \leq 3$V, the function $\tau_0^{(R)}$ varies over three orders of magnitude, and $\tau_0^{(P)}$ varies over one decade. Furthermore the energy shifts δE are non-linear functions of V_{gs}.

Microscopic physical or phenomenological models for the electronic band and defect energies, such as the double well (DW) or the non-radiative multiphonon (NMP) model [2], [3], analyze the stress-voltage dependence of the transitions of single defects. The first one is a two-state model suitable for the more permanent defects. The latter one takes into account phonon-assisted transitions via two further metastable states and then projects onto the stable states to obtain τ_c, τ_e for the recoverable oxide traps. Based on experimental data, the parameter extraction for these two models generates a characteristic defect database [15]. We parametrize the inputs of our modeling according to the detailed experimental MSM data obtained for an example technology.

Analyzing the defect database, we determine the parameters $V_{\text{gs}} \mapsto \tau_0$, $V_{\text{gs}} \mapsto \delta E$ and $(e_c, e_e) \mapsto \Phi$ of our analog modeling. Therefore, the present approach includes the non-trivial two-stage dynamics of the NMP defects. To be specific, we fit the database information for each defect type r to a Gaussian distribution map

$$\Phi_r(e_c, e_e) = \frac{\alpha_r}{\sqrt{\det(2\pi C_r)}} \ \exp\left(-\frac{1}{2}\begin{pmatrix} e_c \\ e_e \end{pmatrix}^t C_r^{-1} \begin{pmatrix} e_c \\ e_e \end{pmatrix}\right) \tag{4}$$

with a symmetric 2×2 covariance C_r and a scaling factor α_r, this map then enters eq. (2).

Fixing the energy space point (e_c, e_e), the capture-emission process $w_{e_c,e_e,V_{\text{gs}}}^{(r)}(t)$ in (2) satisfies the ordinary differential equation (1), which we rewrite here to

$$\dot{w}(t) = a(t)w(t) + b(t), \quad w(t_0) = w_0, \tag{5}$$

with

$$a(t) = -\left(\frac{1}{\tau_e} + \frac{1}{\tau_c}\right)(t) < 0, \quad b(t) = \frac{1}{\tau_c(t)} \geq 0. \tag{6}$$

Its coefficients a, b acquire the time dependence of V_{gs} and take continuous values. Hence, $w_{e_c,e_e,V_{\text{gs}}}^{(r)}(t)$ is a function of the stress history $\{V_{\text{gs}}(s) : t_0 \leq s \leq t\}$.

The next section of this paper analyzes the solution to this differential equation, where the ratio

$$\left(-\frac{b}{a}\right)(t) = \left(\frac{\tau_e}{\tau_c + \tau_e}\right)(t) > 0 \tag{7}$$

will be of interest.

III. Solution to the Differential Equation

The solution to the differential equation (5) reads

$$w(t) = P_1(t, t_0)w(t_0) + P_2(t, t_0) \tag{8}$$

with

$$P_1(t_2, t_1) = \exp\left(+\int_{t_1}^{t_2} \mathrm{d}s \ a(s)\right), \tag{9}$$

$$\begin{aligned} P_2(t_2, t_1) &= \int_{t_1}^{t_2} \mathrm{d}s \ b(s) \exp\left(+\int_s^{t_2} \mathrm{d}r \ a(r)\right) \\ &= \int_{t_1}^{t_2} \mathrm{d}s \ b(s) P_1(t_2, s). \end{aligned} \tag{10}$$

We have $0 < P_1(t_2, t_1) \leq 1$ as well as $0 \leq P_2(t_2, t_1)$ for all $t_2 \geq t_1$, and $P_2(t, t) = 0$.

A. Composition property of the solution

The following composition property

$$P_1(t_3, t_2) \ P_1(t_2, t_1) = P_1(t_3, t_1), \tag{11}$$

$$P_1(t_3, t_2) \ P_2(t_2, t_1) + P_2(t_3, t_2) = P_2(t_3, t_1) \tag{12}$$

for $t_3 \geq t_2 \geq t_1 \geq t_0$ will be of central interest. We conveniently rewrite it in matrix notation as

$$P(t_3, t_1) = P(t_3, t_2) P(t_2, t_1), \tag{13}$$

where

$$P(t_2, t_1) := \begin{pmatrix} P_1(t_2, t_1) & P_2(t_2, t_1) \\ 0 & 1 \end{pmatrix} \tag{14}$$

denotes a matrix-valued function of time. The solution $w(t)$ to the ODE is recovered via

$$\begin{pmatrix} w(t) \\ 1 \end{pmatrix} = P(t, t_0) \begin{pmatrix} w(t_0) \\ 1 \end{pmatrix} \tag{15}$$

and entirely determined by $P(t, t_0)$ and the initial condition.

B. Solution in case of periodic stress voltage

Let be $V_{\text{gs}}(t + T) = V_{\text{gs}}(t)$ for some period $T > 0$ and all times $t \geq t_0$. The coefficient functions of the ODE (5) inherit this periodicity, $a(T + t) = a(t)$, $b(T + t) = b(t)$ for all $t \geq t_0$. As a consequence, we have the key property

$$P(t_2 + T, t_1 + T) = P(t_2, t_1). \tag{16}$$

Therefore, the solution w of the ODE at time $t = t_0 + nT + r$ with $n \in \mathbb{N}_0$ and $r \geq 0$ is determined by

$$\begin{aligned} P(t_0 + nT + r, t_0) &= P(t_0 + nT + r, t_0 + nT) \ P(t_0 + nT, t_0) \\ &= P(t_0 + r, t_0) \ P(t_0 + T, t_0)^n, \end{aligned} \tag{17}$$

where we have used the composition rule and the periodicity.

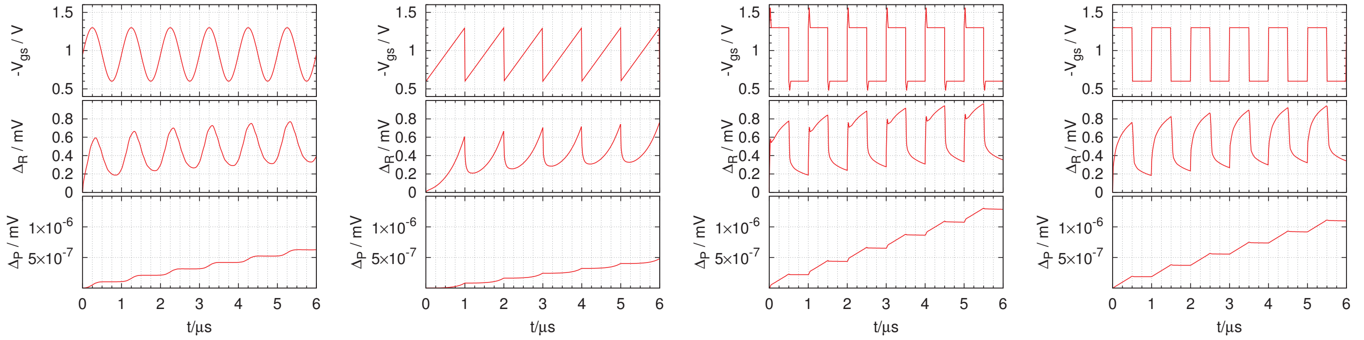

Figure 1. Comparison of the single-transistor short-term NBTI degradation for different stress patterns: sine, sawtooth, digital with overshoots, digital w/o overshoots (left to right), at $\vartheta = 170\,°\mathrm{C}$, $f = 1\,\mathrm{MHz}$. The time axis is in units of the period $T = 1\mu\mathrm{s}$. The stress signal (top) causes a "recoverable" threshold voltage shift Δ_R (mid plot) and a "permanent" shift Δ_P (bottom). In the above plots, the contribution Δ_P is far beyond any experimental detectability and depicted here merely for theoretical considarations, illustrating its intra-period variation and monotonicity in t.

In the calculation of the factor $P(t_0+T,t_0)^n$ we define the shorthands $A := P_1(t_0+T,t_0)$, $B := P_2(t_0+T,t_0)$ and find

$$P(t_0+T,t_0)^n = \begin{pmatrix} A^n & \sum_{j=0}^{n-1} A^j B \\ 0 & 1 \end{pmatrix} = \begin{pmatrix} A^n & \frac{1-A^n}{1-A} B \\ 0 & 1 \end{pmatrix}. \quad (18)$$

The first equality follows by induction, the second one by use of the geometric series.

After multiples of the period T, the solution to the initial value $w(t_0)$ is

$$w(nT+t_0) = \left(w(t_0) - \frac{B}{1-A} \right) A^n + \frac{B}{1-A}, \quad (19)$$

i.e. decays exponentially to a saturation value $B/(1-A)$, which is characterized by an equilibrium between capture and emission over one stress period. Therefore, also the threshold voltage shift saturates at large times. Notice that for $T > 0$, always $|A| < 1$. At large times, the system looses information about its initial condition $w(t_0)$,

$$\lim_{n\to\infty} P(t_0+T,t_0)^n = \begin{pmatrix} 0 & \frac{B}{1-A} \\ 0 & 1 \end{pmatrix}, \quad (20)$$

i.e. the $(1,1)$ matrix element vanishes.

In summary, the solution to the initial value problem (5) is given by

$$\begin{pmatrix} w(t) \\ 1 \end{pmatrix} = P(t_0+r,t_0) \begin{pmatrix} A^n & \frac{1-A^n}{1-A} B \\ 0 & 1 \end{pmatrix} \begin{pmatrix} w(t_0) \\ 1 \end{pmatrix}. \quad (21)$$

Digital-stress studies [5], [6], [7] calculate the involved integrals analytically. For arbitrary analog stress patterns, a numerical integration is necessary though.

IV. Numerical Evaluation

The solution (21) to the ODE (5) at time $t = t_0 + nT + r$, $n \in \mathbb{N}_0$, admits without loss of generality $0 \le r < T$. Therefore, the functions

$$[0,T] \ni t \mapsto P_j(t_0+t,t_0), \qquad j = 1,2, \quad (22)$$

provide complete knowledge about the NBTI degradation at any $t > t_0$, including large t, for a fixed periodic stress pattern. We calculate these functions numerically via a discretization of the time interval $[0,T]$ and suitable spline interpolation of the discrete data.

To this end, we fully evaluate the double integral in P_2 without any approximation, such as that of a constant integrating factor [12], and therefore have no restriction to a class of high-frequency stress signals. With the aging parameters that we extracted for an example technology, a 1MHz sine stress for instance violates the applicability criterion of the constant integrating factor, $P_1(T,0) \approx 1$, for a non-negligible part of recoverable defects. Furthermore, lower-frequency signals lead to a stronger violation.

Our numerical algorithm consists of two parts: In the first step, the functions P_1, P_2 are calculated on a grid that discretizes $[0,T]$. This grid adapts to the specific properties of the stress signal, such as the singular points of V_{gs}. Performing the involved time integrations is numerically efficient since they extend over (subintervals of) $[0,T]$, even for operation times t that are several orders of magnitude larger than T. The time integrands themselves cover a range of several orders of magnitude. Therefore, special care in the numerical integration and interpolation procedures is necessary in order to overcome a number of numeric subtleties and to retain numerical precision in the calculation of the solution.

The second step calculates the threshold voltage shifts at arbitrary observation times by means of (21) and the previously computed data, this step is numerically very fast.

We couple the model to the Cadence Spectre electric circuit simulator via the URI framework, allowing in particular the simulation of long-term circuit aging and the lifetime studies of the analog behavior of a circuit design.

The present method enables us to study the implications of different analog-stress wave-forms on the short- and long-term NBTI degradation. Our numerical simulation uses a temperature $\vartheta = 170\,°\mathrm{C}$, a stress signal frequency $f = 1\,\mathrm{MHz}$, and continuous stress voltage levels between $V_h = -1.3\,\mathrm{V}$ and $V_l = -0.6\,\mathrm{V}$. Figure 1 compares the short-term NBTI threshold voltage shift caused by four different analog stress signals. Whereas the degradation due to the "recoverable" defects clearly shows recovery effects during the phases of

low stress voltage, the "permanent" contributions cause a practically always increasing degradation. Quantitative details strongly depend on the stress pattern.

Figure 2 (left) contrasts the long-term NBTI threshold voltage shift of these stress patterns. At smaller operation times t, the recoverable defects dominate $\Delta(t)$. However, the contribution of the "recoverable" component levels off at large times $t \gtrsim 10^4$s, with the level determined by the limit (20). As a consequence, a crossover to the dominance of permanent defects occurs at times $t \approx 10^2$s and manifests in a kink in $\Delta(t)$. This kink prevents the direct extrapolation of $\Delta(t)$ from experimental data obtained over a small interval of stress times $t \lesssim 10^0$s to the time domain where the permanent defects become important, this fact was clearly expected because of the different natures of the two microscopic mechanisms. Since our modeling accounts for both defect types, we have access to the large-time degradation. The same leveling-off as before occurs also for the "permanent" component, but at time scales beyond typical experimental observation times.

The quantitative details of the $\Delta(t)$ shape can be highly stress waveform dependent because different stress patterns stimulate the NBTI defects in different ways and for instance have different saturation levels in (20). The non-trivial crossings between the degradation due to a sawtooth signal and the ones due to a sine or square-wave stress illustrates this stress-pattern sensitivity.

The contribution of the individual defect to the degradation saturates exponentially in time, eq. (19). On the other hand, we find that in the pre-saturation regime $10^3\text{s} \lesssim t \lesssim 10^7\text{s}$ the statistical average $\Delta(t)$ over all defects is close to a power-law time dependence t^n, with the exponent taking values $n = 0.1 \ldots 0.25$. Such a power law is frequently observed in NBTI experiments [16] and widely used as an effective NBTI model. In the indicated window of observation times t, the exponent n slightly decreases with increasing time, thus foreshadowing the saturation at very large t.

Adding overshoots to an AC signal introduces a new time interval with a strong degradation and also one with a strong recovery, see the two plots on the right in Fig. 1. Compared to the digital AC stress (dashed line in Fig. 2, left), the new degradation effects outweigh the recovery in the given example (dash-dotted line) and lead to an enhancement of the NBTI degradation. At $t = 10^7$s, the shift $\Delta(t)$ increases by 4% due to the overshoots.

Figure 2 (right) studies the influence of the intra-period time position at which long-time shifts $\Delta(t)$ are evaluated. The intra-period variation originates to a large extent from the recoverable defects. Comparing to the averaged inter-period value of $\Delta(t)$, the intra-period amplitude is rather small at large operation times.

We now proceed from the analysis of the single-transistor degradation to the analog NBTI simulation of a circuit. For this purpose, we use a seven stages ring oscillator (Fig. 3) in a 130 nm predictive technology[1]. In this circuit, the PMOS devices involved in the inverters and in the NAND gate are susceptible to NBTI degradation, and their threshold voltage shift results in a decrease of the oscillation frequency.

[1]We use the PTM data provided by the NIMO group at Arizona State University.

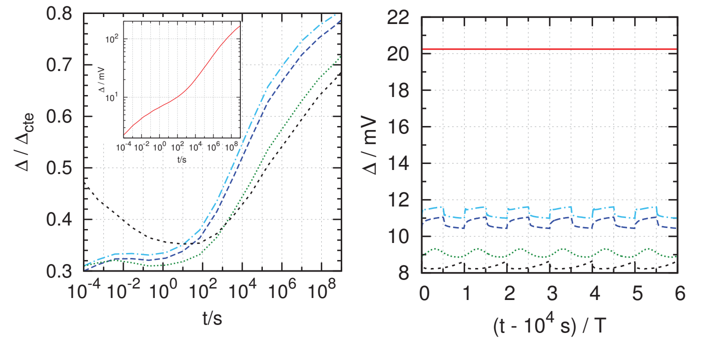

Figure 2. Single-transistor long-term NBTI degradation $\Delta(t)$ for the stress patterns of Fig. 1: time-constant stress (solid line), digital with overshoots (dash-dots), digital (long dashes), sine (dots), and sawtooth (short dashes). *Left:* The shift $\Delta(t)$ over a wide range of operation times t, divided by the shift $\Delta_{\text{cte}}(t)$ caused by a time-constant stress. In the plot, $\Delta(t)$ is evaluated at the beginning of the stress periods. The inset shows the shift $\Delta_{\text{cte}}(t)$ for reference. Operation times around 10^8s correspond to the NBTI simulation of 10^{14} stress periods and pose numerically no problem. *Right:* Intra-period variation of $\Delta(t)$ during 6 stress periods, after having operated the device for 10^4s.

t	$\Delta(t)$ / mV	f / GHz	f shift
0	0	2.185	0
10^2 s	2.9	2.183	−0.09 %
1 day	15	2.175	−0.5 %
1 month	39	2.157	−1.3 %
1 year	66	2.136	−2.2 %

Table I. NBTI aging simulation for a ring oscillator in 130 nm predictive technology at $\vartheta = 170\,°$C. The table shows the NBTI threshold voltage shift $\Delta(t)$ of the involved pFET devices at several operation times t of the circuit. This shift induces a lowering in the oscillation frequency f, as compared to its "fresh" value at $t = 0$.

We couple the analog NBTI modeling to the Spectre electric circuit simulation. All pFETs see approximately the same (but phase-shifted) stress voltage (top-mid plot in Fig. 3). Since the stress $V_{\text{gs}} \approx 0$ during half of the period, recovery effects become important. The NBTI shift $\Delta(t)$ over a wide range of operation times (right plot) exhibits the same structure of a crossover from recoverable to permanent defects as observed in Fig. 2. At times $t \gtrsim 10^3$s, the permanent defects dominate the NBTI degradation. Taking into account the threshold voltage shift during the electric circuit simulation we obtain the change in the oscillation frequency as given in Tab. I.

V. Relation to digital-AC NBTI modelings

In the special case of digital stress signals $V_{\text{gs}}(t) \in \{V_h, V_l\}$, the analog modeling approach reproduces the predictions of existing digital-AC modelings [5], [6], [7]:

Let $w^{\infty}_{h,l} := \left(\frac{\tau_e}{\tau_c+\tau_e}\right)(V_{h,l})$ denote the equilibrium occupation probability of a fixed defect at high or low stress, respectively, with $\tau_{c,e}(V_{\text{gs}})$ given by (3). The digital-stress capture-emission process $w(t)$ with $w(t_0) = w^{\infty}_l$ then has

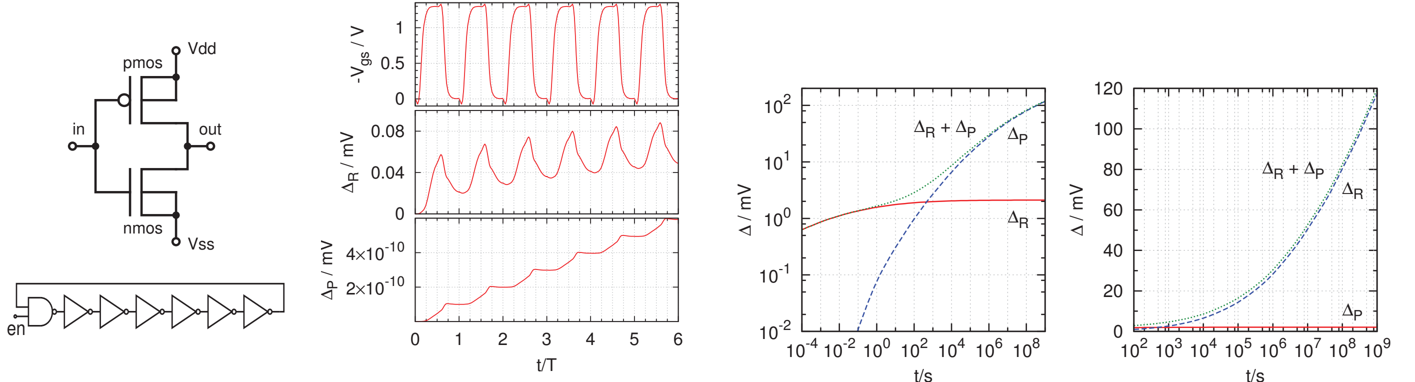

Figure 3. Analog circuit-level NBTI simulation for a ring oscillator in a predictive technology ($\vartheta = 170\,°\mathrm{C}$). *Left:* Oscillator with 7 stages (1 NAND gate, 6 inverters). The inverter uses a PMOS and an NMOS device. *Mid*: Time-dependent gate-source voltage (top) and recoverable and permanent NBTI degradation (mid and bottom) during six oscillation periods. All pMOSFETs see approximately the same (but phase-shifted) stress voltage. The short-time degradation patterns (mid and bottom) are different from those of an idealized circuit that switches strictly between only two voltage levels. *Right (2 plots):* The long-time circuit-level NBTI simulation quantitatively confirms a comparatively small Δ_R at large operation times, where the degradation is mainly due to the permanent defects. The rightmost plot zooms into the region of large operation times t. Table I indicates the corresponding shift in the oscillation frequency.

the form

$$w(t) = w_l^\infty + (w_h^\infty - w_l^\infty)\ h_{\tau_h,\tau_l}(t). \tag{23}$$

Here, τ_h and τ_l denote the characteristic decay times at high or low stress, $1/\tau_{h,l} = 1/\tau_c(V_{h,l}) + 1/\tau_e(V_{h,l})$. The function h_{τ_h,τ_l} depends on the specific sequence of switching the stress between V_h and V_l.

Inserting (23) into (2) and changing variables from (e_c, e_e) to (τ_h, τ_l) yields the main term

$$\int \mathrm{d}e_c \mathrm{d}e_e\ \Phi(e_c, e_e)\ (w_h^\infty - w_l^\infty)\ h_{\tau_h,\tau_l}(t) = \int \mathrm{d}\tau_h \mathrm{d}\tau_l\ g(\tau_h, \tau_l)\ h_{\tau_h,\tau_l}(t). \tag{24}$$

Thus, the CET map reads

$$g(\tau_h, \tau_l) = \Phi(e_c, e_e) \times (w_h^\infty - w_l^\infty) \times D, \tag{25}$$

with the Jacobian

$$D = \left|\frac{\partial(\tau_h, \tau_l)}{\partial(e_c, e_e)}\right| = \beta^2 \tau_h^2 \tau_l^2 \left(\frac{1}{\tau_c(V_h)\tau_e(V_l)} - \frac{1}{\tau_e(V_h)\tau_c(V_l)}\right). \tag{26}$$

The NBTI information encoded in $g(\tau_h, \tau_l)$ is limited to the class of two-level stress signals that switch between V_h and V_l. The present parametrization specializes to this case by eqns. (25) and (3).

The factor $w_h^\infty - w_l^\infty$ in g suppresses all defects which do not have $\tau_c(V_l) \gg \tau_e(V_l)$ and $\tau_e(V_h) \gg \tau_c(V_h)$, such that the subsequent approximation $\tau_c(V_l), \tau_e(V_h) \to \infty$ may apply, which results in $\tau_h \approx \tau_c(V_h)$, $\tau_l \approx \tau_e(V_l)$ and $D \approx \beta^2 \tau_h \tau_l$.

VI. Conclusions

The present model makes the NBTI circuit-level aging simulation available to analog design. Its explicit solution given for arbitrary operation times, which need not be multiples of the stress period T, allows a detailed control of the short-term as well as of the long-term threshold voltage shift. Since the numeric solution can be implemented efficiently, the model can be directly integrated into electronic circuit simulators. We have demonstrated its application to circuit design by the analog simulation of a ring oscillator.

Acknowledgments

We thank Ben Kaczer for a worthwhile exchange of ideas. KUG, CS and RJ furthermore thank André Lange and Leif Müller for valuable discussions.

This project has received funding from the European Union's Seventh Framework Programme for research, technological development and demonstration under grant agreement no. 619234 (MoRV).

References

[1] V. Huard, M. Denais, and C. Parthasarathy, "NBTI degradation: From physical mechanisms to modelling," *Microel. Rel.*, vol. 46, no. 1, pp. 1–23, 2006.

[2] T. Grasser, B. Kaczer, W. Goes, T. Aichinger, P. Hehenberger, and M. Nelhiebel, "Understanding negative bias temperature instability in the context of hole trapping," *Microel. Eng.*, vol. 86, no. 7–9, pp. 1876–1882, 2009.

[3] T. Grasser, "Stochastic charge trapping in oxides: From random telegraph noise to bias temperature instabilities," *Microel. Rel.*, vol. 52, no. 1, pp. 39–70, 2012.

[4] T. Grasser, Ed., *Bias Temperature Instability for Devices and Circuits*. Springer, 2014.

[5] H. Reisinger, T. Grasser, W. Gustin, and C. Schlunder, "The statistical analysis of individual defects constituting NBTI and its implications for modeling DC- and AC-stress," in *Proc. IRPS*, 2010, pp. 7–15.

[6] H. Reisinger, T. Grasser, K. Ermisch, H. Nielen, W. Gustin, and C. Schlunder, "Understanding and modeling AC BTI," in *Proc. IRPS*, 2011, p. 6A.1.1.

[7] G. Wirth, R. da Silva, and B. Kaczer, "Statistical Model for MOSFET Bias Temperature Instability Component Due to Charge Trapping," *IEEE Trans. El. Dev.*, vol. 58, no. 8, p. 2743, 2011.

[8] T. Grasser, P. J. Wagner, H. Reisinger, T. Aichinger, G. Pobegen, M. Nelhiebel, and B. Kaczer, "Analytic modeling of the bias temperature instability using capture/emission time maps," in *Proc. IEDM*, 2011, p. 27.4.1.

[9] C. Yilmaz, L. Heiß, C. Werner, and D. Schmitt-Landsiedel, “Modeling of NBTI-recovery effects in analog CMOS circuits,” in *Proc. IRPS*, 2013, p. 2A.4.

[10] L. Heiß, “Modeling and Simulation of NBTI in Analog CMOS Circuits,” Master’s thesis, TU München, 2012.

[11] F. Alagi, “A study of the interface-trap activation kinetics in the Negative Bias Temperature Instability,” *Microel. Rel.*, vol. 54, no. 1, pp. 22–29, 2014.

[12] F. Alagi, M. Rossetti, R. Stella, and E. Viganò, “A reversible first-order dispersive model of parametric instability,” *Microel. Rel.*, vol. 54, no. 3, pp. 561–569, 2014.

[13] P. Weckx, B. Kaczer, M. Toledano-Luque, T. Grasser, P. Roussel, H. Kukner, P. Raghavan, F. Catthoor, and G. Groeseneken, “Defect-based methodology for workload-dependent circuit lifetime projections - Application to SRAM,” in *Proc. IRPS*, 2013, p. 3A.4.1.

[14] G. Pobegen and T. Grasser, “On the Distribution of NBTI Time Constants on a Long, Temperature-Accelerated Time Scale,” *IEEE Trans. El. Dev.*, vol. 60, no. 7, pp. 2148–2155, 2013.

[15] G. Rzepa, W. Goes, G. Rott, K. Rott, M. Karner, C. Kernstock, B. Kaczer, H. Reisinger, and T. Grasser, “Physical Modeling of NBTI: From Individual Defects to Devices,” in *Proc. SISPAD*, 2014, pp. 81–84.

[16] A. Kerber, S. Krishnan, and E. Cartier, “Voltage Ramp Stress for Bias Temperature Instability Testing of Metal-Gate/High- k Stacks,” *IEEE El. Dev. Let.*, vol. 30, no. 12, pp. 1347–1349, 2009.